A fluorescent timer reporter enables sorting of insulin secretory granules by age

Received for publication, January 5, 2020, and in revised form, March 21, 2020 Published, Papers in Press, April 27, 2020, DOI 10.1074/jbc.RA120.012432

Belinda Yau[1,2], Lori Hays[3], Cassandra Liang[4], D. Ross Laybutt[4,5], Helen E. Thomas[6,7], Jenny E. Gunton[8,9], Lindy Williams[8,10], Wayne J. Hawthorne[8,10], Peter Thorn[1,11], Christopher J. Rhodes[12,13], and Melkam A. Kebede[1,2*]

From the [1]Charles Perkins Centre, the [2]School of Life and Environmental Sciences, Faculty of Science, the [8]Faculty of Medicine and Health, and the University of Sydney, Sydney, New South Wales, Australia, the [3]STEM-Department of Biology, Edmonds Community College, Lynnwood, Washington, USA, the [4]Garvan Institute of Medical Research, Sydney, New South Wales, Australia, [5]St. Vincent's Clinical School, University of New South Wales Sydney, Sydney, New South Wales, Australia, [6]St. Vincent's Institute, Fitzroy, Victoria, Australia, the [7]Department of Medicine, St. Vincent's Hospital, University of Melbourne, Fitzroy, Victoria, Australia, the [9]Westmead Institute for Medical Research, University of Sydney, Westmead, New South Wales, Australia, the [10]National Pancreas and Islet Transplant Unit (NPITU), Westmead Hospital, Sydney, New South Wales, Australia, the [11]Discipline of Physiology, School of Medical Sciences, Faculty of Medicine and Health, Charles Perkins Centre, University of Sydney, Camperdown, Australia, [12]Research and Early Development, Cardiovascular, Renal and Metabolic Diseases, BioPharmaceuticals R&D, AstraZeneca Ltd, Gaithersburg, Maryland, USA, and [13]Pacific Northwest Research Institute, Seattle, Washington, USA

Edited by Phyllis I. Hanson

Within the pancreatic β-cells, insulin secretory granules (SGs) exist in functionally distinct pools, displaying variations in motility as well as docking and fusion capability. Current therapies that increase insulin secretion do not consider the existence of these distinct SG pools. Accordingly, these approaches are effective only for a short period, with a worsening of glycemia associated with continued decline in β-cell function. Insulin granule age is underappreciated as a determinant for why an insulin granule is selected for secretion and may explain why newly synthesized insulin is preferentially secreted from β-cells. Here, using a novel fluorescent timer protein, we aimed to investigate the preferential secretion model of insulin secretion and identify how granule aging is affected by variation in the β-cell environment, such as hyperglycemia. We demonstrate the use of a fluorescent timer construct, syncollin-dsRedE5TIMER, which changes its fluorescence from green to red over 18 h, in both microscopy and fluorescence-assisted organelle-sorting techniques. We confirm that the SG-targeting construct localizes to insulin granules in β-cells and does not interfere with normal insulin SG behavior. We visualize insulin SG aging behavior in MIN6 and INS1 β-cell lines and in primary C57BL/6J mouse and nondiabetic human islet cells. Finally, we separated young and old insulin SGs, revealing that preferential secretion of younger granules occurs in glucose-stimulated insulin secretion. We also show that SG population age is modulated by the β-cell environment *in vivo* in the *db/db* mouse islets and *ex vivo* in C57BL/6J islets exposed to different glucose environments.

The pancreatic β-cell plays a central role in glucose homeostasis, and β-cell dysfunction is key to the pathogenesis of type 2 diabetes. This manifests mainly as a reduction in glucose-stimulated insulin secretion (GSIS). In β-cells, insulin is stored in secretory granules (SGs), and in response to stimulation, SGs mobilize and fuse with the plasma membrane, delivering insulin to the bloodstream. Models of sequential secretion, in which SGs are targeted for secretion based on their proximity to the plasma membrane, have been considered for many years (1–3). However, the discovery of "newcomer" insulin SG (4), "kiss-and-run" dynamics (5, 6), compound insulin SG secretion (7), and complexities surrounding the relationship between SG docking and exocytosis (8) suggests that either multiple or more intricate mechanisms dictate SG selection for GSIS.

Granule aging represents another facet of SG selection for insulin secretion. Evidence accumulating over the last 30 years, including pulse-chase radiolabeling as early as the 1960s (9–11), suggests that the age of SGs may play a significant role in dividing SGs into functionally distinct pools. More recently, fluorescent marker techniques such as the TMR-Star have allowed high-resolution imaging of these uniquely aged pools (9, 12–16). In parallel, it was observed that upon glucose stimulation, a highly mobile pool of SG rapidly moves from the interior of the β-cell to be secreted with minimal to no residence time at the plasma membrane (17, 18). This pool of SGs has been referred to as the "newcomer" or "restless" SG pool and is thought to account for all of the second phase of GSIS and a substantial portion of first phase GSIS (19, 20). Since then, characterization of young SGs using fluorescent marker techniques has revealed that they are composed of newly synthesized insulin, exhibit high mobility (14, 15), and may account for this newcomer pool. Interestingly, in direct contrast to the classical model, recent studies have shown that aged SGs, including those that are predocked, lose mobility and fusion competency as a function of age (14).

In β-cells, insulin is produced as a precursor, proinsulin, which is processed to mature insulin (8). Mature insulin combines with Zn^{2+} and forms a hexameric crystal within the SGs. These SGs can be stored for days in the cytosol, and the estimated half-life of insulin SGs is 3–5 days (21). On average, a functional β-cell contains ~10,000 SGs (22, 23). In response to

This article contains supporting information.

* For correspondence: Melkam Kebede, melkam.kebede@sydney.edu.au.

a single stimulus, a very small percentage of these insulin SGs (1–5% of total insulin content, often less, over the course of an hour) are released through exocytosis. Older insulin SGs that do not undergo exocytosis are targeted to the lysosome for degradation (21, 24), but how a cell can distinguish young SGs from old is unclear. Interestingly, under conditions of metabolic stress, β-cells could potentially lose their ability to distinguish young SGs from old; in diabetes, β-cells hypersecrete insulin to compensate for insulin resistance and eventually become degranulated (25–27). Whether these changes are intrinsic to the SG or regulated by the β-cell environment is not defined.

The use of fluorescent timer proteins, such as DsRed-E5 (28), to segregate vesicles by age has been previously demonstrated in bovine chromaffin cells (13) and in PC12 neuroendocrine cells (29). In both studies, preferential secretion of younger pools of vesicles was identified. Moreover, age-distinct vesicle pools identified in these studies were found not only to display dissimilar motility and localization, but also to differentially respond to secretagogue challenges (13).

In the present study, we aimed to characterize young and old pools of insulin granules and investigate their behaviors in a model of type 2 diabetes. We employed an established fluorescent timer (28) construct that is targeted within the lumen of insulin SG, syncollin-dsRedE5TIMER (30), to visualize insulin SGs as a function of age. The dsRedE5TIMER is a coral fluorescent protein that changes its emission characteristics from a green 505–550 nm to a red 590–700 nm with time. Therefore, the green/red fluorescence ratio indicates the age of the protein, and a yellow-orange fluorescence results from dsRedE5TIMER protein in an intermediate state of folding, reflective of a "middle-aged" granule (28). Syncollin is a soluble intragranular protein, which is not normally expressed in β-cells. However, when syncollin is tagged with a fluorescent protein, it is exclusively targeted to the lumen of β-cell granules (31). Using this syncollin-dsRedE5TIMER adenoviral construct, we have successfully expressed the protein in β-cell granules (30). Here, we show fluorescent timer maturation from green to red in the mouse MIN6 pancreatic β-cell line, in the INS1 insulinoma rat β-cell line, and in primary mouse and human pancreatic islet cells. We demonstrate that insulin SGs differentially localize within the β-cell cytoplasm by age, with younger ISGs positioned closer to the plasma membrane. Moreover, using flow cytometer–assisted organelle sorting (FAOS) analysis (32, 33), we identify age-distinct populations of insulin SGs while excluding large multigranular bodies and establish that younger insulin SG selection is a glucose-mediated phenomenon. Finally, with islets from WT and obese type 2 diabetic *db/db* mice, we show that the granule population age is regulated by the β-cell environment under conditions of chronic metabolic stress.

Results

Syncollin-dsRedE5TIMER targets insulin SGs and differentiates younger and older SG populations

Acquisition of a 10-nm-step excitation λ scan in adenovirus syncollin-dsRedE5TIMER–infected dispersed mouse primary islets, 48 h post-infection, identified two distinct excitation peaks at 490 and 570 nm corresponding to dsRed-E5 protein's expected immature green, then mature red, fluorescence wavelengths, respectively (Fig. 1*A*). As with previous studies employing fluorescent timer constructs (34), a single excitation of 490 nm was used to minimize photobleaching, with sequential detection of 505–550 nm and 590–700 nm bands used to capture the immature and mature forms of dsRed-E5, respectively.

By confocal microscopy, transduction of syncollin-dsRedE5TIMER into β-cells and dispersed islets clearly resulted in fluorescent punctate granule-like structures within the cytoplasm of cells (Fig. 1*B*). As previously shown in both a rat insulinoma β-cell line and in primary rat islets, adenovirus induced expression of fluorescently labeled syncollin leads to its targeting to the insulin SG lumen within β-cells (30, 31). To confirm these findings in mice, we stained the MIN6 mouse insulinoma cell line with a guinea pig anti-insulin antibody 24, 48, and 72 h post-transduction with syncollin-dsRedE5TIMER (Fig. 1*B*). It was apparent that although not all insulin SG expressed syncollin-dsRedE5TIMER, colocalization of insulin and dsRed-E5 fluorescence was clear, with a Mander's overlap coefficient of 0.917 ± 0.033 S.E. and 0.920 ± 0.034 for immature and mature forms of syncollin-dsRedE5TIMER, respectively, by 48 h (Fig. 1*C*).

To further confirm the presence of syncollin-dsRedE5TIMER in mouse insulin SGs, we performed sucrose gradient subcellular fractionation of syncollin-dsRedE5TIMER–infected MIN6 cells at 72 h post-transduction and demonstrated that syncollin and insulin co-fractionated in compartments positive for granule markers Vamp8 and PCSK2, but not β-actin (Fig. 1, *D* and *E*). Additionally, to ensure that syncollin-dsRedE5TIMER expression was compatible with β-cell function, we performed GSIS assays in syncollin-dsRedE5TIMER–infected MIN6 cells 72 h post-infection and confirmed high-glucose–stimulated secretion of syncollin alongside PCSK2 (Fig. 1*F*). We additionally performed GSIS in primary dispersed mouse islets with and without syncollin-dsRedE5TIMER infection, to confirm that insulin secretion and content were not affected by adenovirus transduction of the syncollin construct (Fig. 1*G*).

To characterize the dynamics of syncollin-dsRedE5TIMER within insulin SGs, dispersed primary islet cells from normal C57BL/6J mice and nondiabetic human organ donors were infected to observe over a 72-h time course. Substantial immature green dsRed-E5 fluorescence was observed by 18 h post-infection, with maturation into red primarily observed as an overlapping yellow (Fig. 1*H*). These yellow granules were termed "middle-aged" SGs, in that they contained the maturing dsRedE5 protein displaying emission at both green and red fluorophores (28). Most interestingly, as new green-fluorescing granules appeared in the β-cell, red older SGs localized in populations within the cell distinct from the younger, newly synthesized granules by 72 h post-transduction (Fig. 1*H*), which appeared to maintain a closer proximity to the plasma membrane. Using fixed TIRF microscopy, we were also able to visualize more green young granules localized to the plasma membrane at 72 h, and not 24 h (Fig. S1).

To address functional dynamics of young and old populations, Brefeldin A was added to syncollin-dsRedE5TIMER–transduced

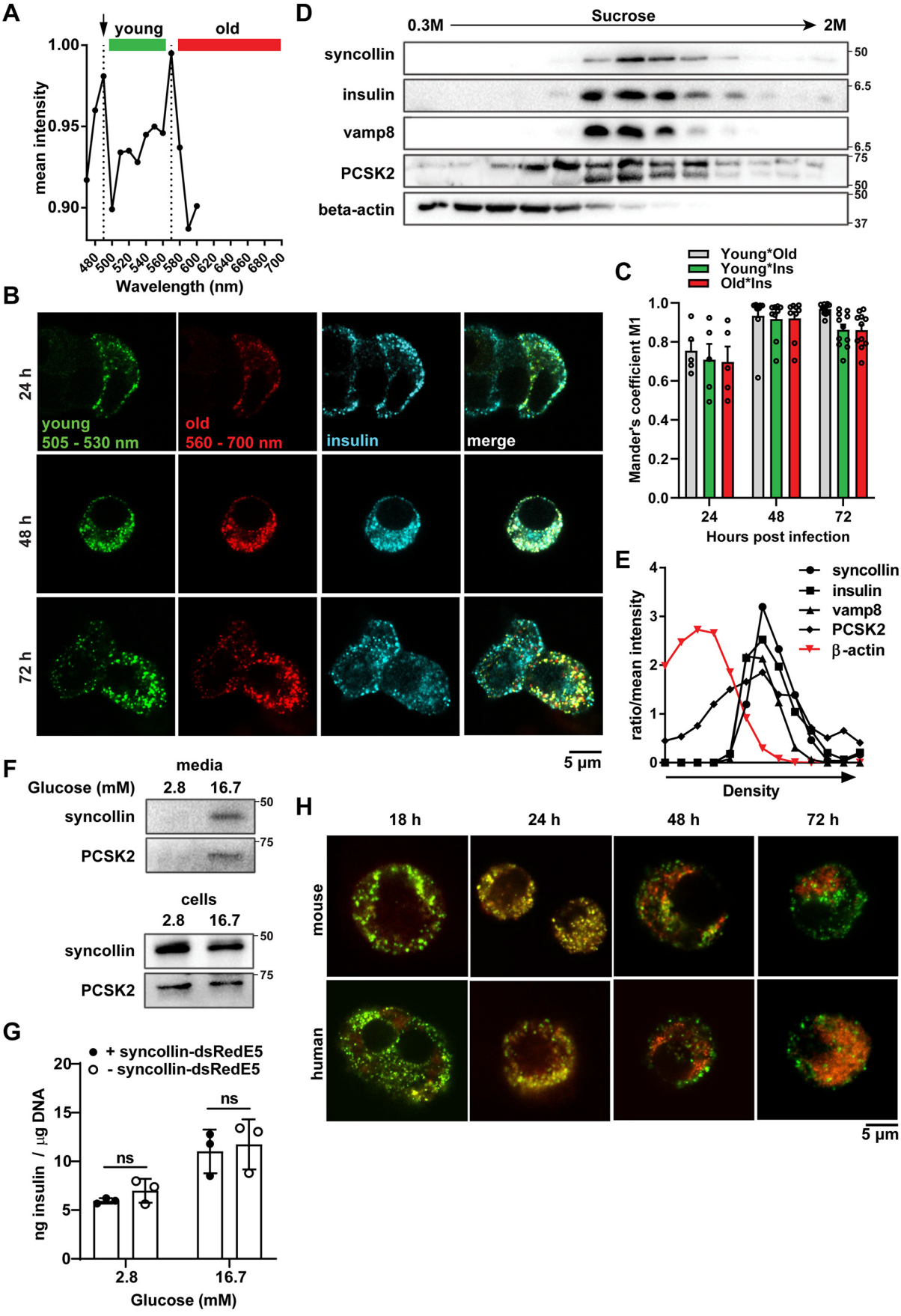
A
young
old
1.00
0.95
0.90
mean intensity
480 500 520 540 560 580 600 620 640 660 680 700
Wavelength (nm)
D
0.3M
Sucrose
2M
syncollin
insulin
vamp8
PCSK2
beta-actin
50
6.5
6.5
75
50
50
37
B
24 h
48 h
72 h
young
505 - 530 nm
old
560 - 700 nm
insulin
merge
5 µm
C
Young*Old
Young*Ins
Old*Ins
Mander's coefficient M1
1.0
0.8
0.6
0.4
0.2
0.0
24
48
72
Hours post infection
E
syncollin
insulin
vamp8
PCSK2
β-actin
ratio/mean intensity
4
3
2
1
0
Density
F
media
Glucose (mM)
2.8
16.7
syncollin
PCSK2
50
75
cells
2.8
16.7
syncollin
PCSK2
50
75
G
+ syncollin-dsRedE5
- syncollin-dsRedE5
ng insulin / µg DNA
20
15
10
5
0
ns
ns
2.8
16.7
Glucose (mM)
H
18 h
24 h
48 h
72 h
mouse
human
5 µm

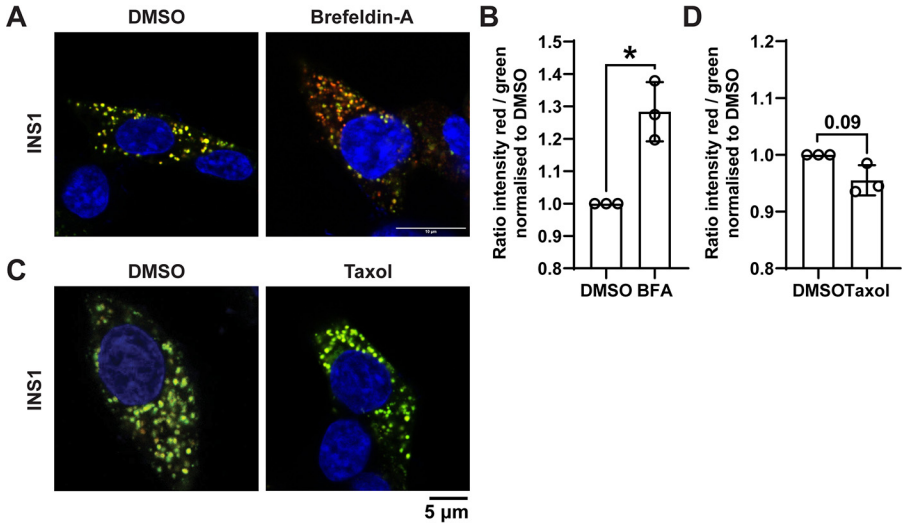

Figure 2. Syncollin-dsRedE5TIMER behavior with brefeldin A and Taxol treatment in INS1 β-cells. *A* and *B*, confocal fluorescence imaging of INS1 cells 48 h post-transduction with syncollin-dsRedE5TIMER, after treatment with 10 μg/ml brefeldin A (*A*) or 5 μM Taxol (*B*) for 3 h at 5.6 mM glucose. *C* and *D*, quantification of green and red fluorescence intensity ratio in brefeldin-A (*C*) or Taxol (*D*) treatments normalized to DMSO control, calculated from an average of 20–30 cells/experiment in three separate experiments. *, $p < 0.05$.

INS1 rat β-cells to halt vesicular transport from Golgi, and this resulted in an observable increase in red fluorescence, corresponding to the loss of SG biogenesis (Fig. 2*A*), and this change in fluorescence ratio was statistically significant (Fig. 2*B*). In contrast, the addition of Taxol to stabilize microtubules resulted in small but nonsignificant increase in green fluorescence, presumably a result of immature SG accumulation due to decreased SG motility and exocytosis (Fig. 2, *C* and *D*). Altogether, these data confirm that syncollin-dsRedE5TIMER transduction of both β-cell models, as well as primary islet cells, results in functionally relevant time-dependent dynamic fluorescence in insulin granules, allowing differentiation of younger and older SG populations for further analyses.

FAOS separates insulin SGs by age

Concurrent with confocal imaging, we used flow cytometry analysis of subcellular particles to characterize our syncollin-dsRedE5TIMER–expressing SGs. FAOS analysis allowed the advantage of measuring both the immature (green) and mature (red) dsRed-E5 fluorescence intensities of individual insulin SGs relative to the entire subcellular particle population. Gating for a typical granule size of 100–500 nm (22) and then single particles (Fig. 3*A*), we aimed to exclude the large multigranular bodies previously measured by Hoboth *et al.* (14) at >500 nm.

Analysis of a time course of fluorescent granules from syncollin-dsRedE5TIMER–transduced mouse islet cells clearly demonstrated the initial expression of immature dsRed-E5 as a distinct green-positive, red-negative granule population at 24 h (green gate). Over 72 h, a gradual shift to red-positive mature dsRed-E5 expression (red gate) is observed, whereas nontransduced control islet cells displayed no fluorescent granules (Fig. 3*B*). By 48 h, numbers of younger green-positive granules appear to be stable, whereas older red-positive granules begin to increase in number from 24 h onward (Fig. 3*C*). Syncollin-dsRedE5TIMER behavior and subsequent FAOS profiles were similar in transduced dispersed human islet cells (Fig. 3*D*). We subsequently expressed these data as a ratio of the old/young granule population percentages, highlighting the increase of the ratio over time (Fig. 3*E*).

Using back-gating analysis, we demonstrated comparable size and scatter properties of both young green-positive granules and aged red-positive granules from primary mouse islet cells 72 h after transduction (Fig. S2*A*). Furthermore, both of these populations also came from gates of comparable size and scatter characteristics as fluorescent particles from INS-1 832/13 GRINCH cells (36) that express hPro-CpepsfGFP within insulin SG but not control INS-1 832/13 cells (Fig. S2, *B* and *C*), as well as intracellularly fluorescently stained insulin particles in MIN6 cells (Fig. S2*D*), further establishing their status as genuine insulin SGs.

Preferential secretion of younger insulin SGs is selective for glucose stimulation

To address the preferential secretion model, we utilized a glucose-stimulated insulin secretion assay immediately followed by FAOS to measure relative populations of young and old SGs within the cell (Fig. 4*A*). 72 h post-transduction with

Figure 1. Characterization of syncollin-dsRedE5TIMER behavior in MIN6 β-cells and primary mouse islets. *A*, λ excitation peak spectra obtained from a 10-nm step acquisition of primary mouse islet cells, 48 h post-transduction with syncollin-dsRedE5TIMER. *Green* and *red colored bars* represent emission detection ranges for young and old granule populations, respectively. Shown is confocal immunofluorescence imaging (*B*) and co-localization analysis (*C*) of young and old granule populations and anti-insulin–stained granules in mouse MIN6 cells at 24, 48, and 72 h post-transduction with syncollin-dsRedE5TIMER. Shown is representative Western blotting (*D*) and representative densitometry analysis (*E*) of syncollin, insulin granule–associated proteins, and β-actin expression after subcellular sucrose fractionation of MIN6 cells, 72 h post-transduction with syncollin-dsRedE5TIMER. *F*, Western blotting of syncollin and prohormone convertase PC2 in MIN6 cells, after 1-h 2.8 mM glucose basal and 1-h 2.8 or 16.7 mM glucose stimulation assay. Medium was precipitated with TFA protein precipitation. *G*, HTRF assay of secreted insulin from dispersed primary mouse islets normalized to DNA content after glucose-stimulated secretion assay, after a 48-h culture with or without transduction of syncollin-dsRedE5TIMER. *H*, confocal fluorescence imaging of primary mouse and human islet cells at 18, 24, 48, and 72 h post-transduction with syncollin-dsRedE5TIMER. *ns*, not significant.

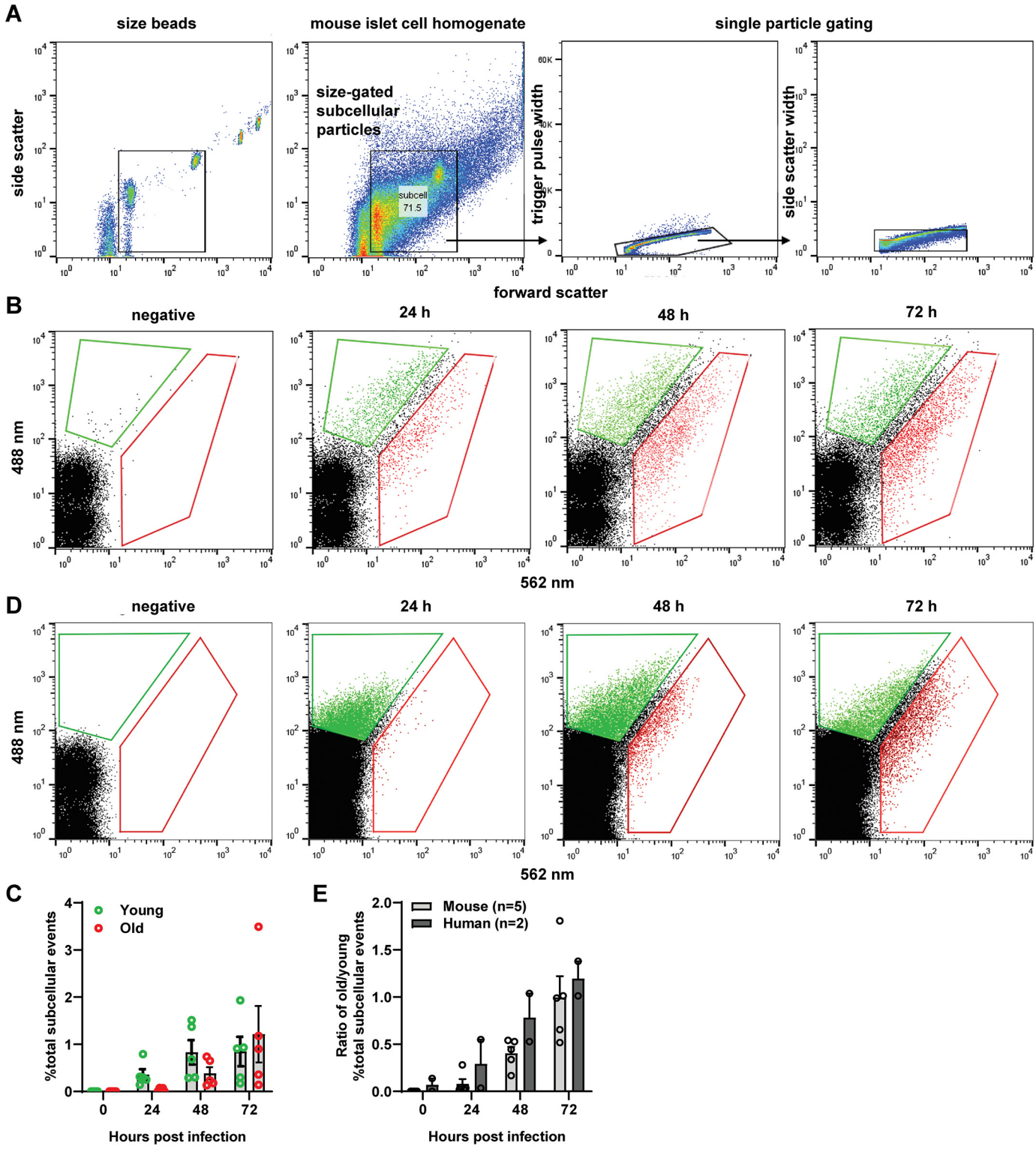

Figure 3. Flow cytometry–assisted organelle sorting of young and old insulin granules in primary mouse and human islets. *A*, representative gating strategy for syncollin-dsRedE5TIMER–positive insulin granules. *First* and *second panels*, BD Biosciences size beads for sub-micron particle size reference, gated for particles between 100 and 500 nm and applied to processed islet cell lysate. *Third* and *fourth panels*, trigger pulse width and side scatter width gating to observe single particles of similar scatter properties. *B* and *C*, FAOS gating strategy applied to dispersed mouse islets (*B*) and human islets (*C*) and then gated for 488- and 562-nm fluorescence at 24, 48, and 72 h post-transduction with syncollin-dsRedE5TIMER. Arbitrary "young" and "old" gates are defined by the first presence of fluorescent particles at 24 h or with total fluorescent population divided along the *diagonal*. All gates are consistent throughout samples for each FAOS experiment. *D*, number of fluorescent particles in defined young and old gates expressed as a percentage of total gated subcellular particles in dispersed mouse islets at 24, 48, and 72 h post-transduction with syncollin-dsRedE5TIMER. *E*, ratio of the percentage of old subcellular particles over the percentage of young subcellular particles in dispersed mouse and human islets at 24, 48, and 72 h post-transduction with syncollin-dsRedE5TIMER.

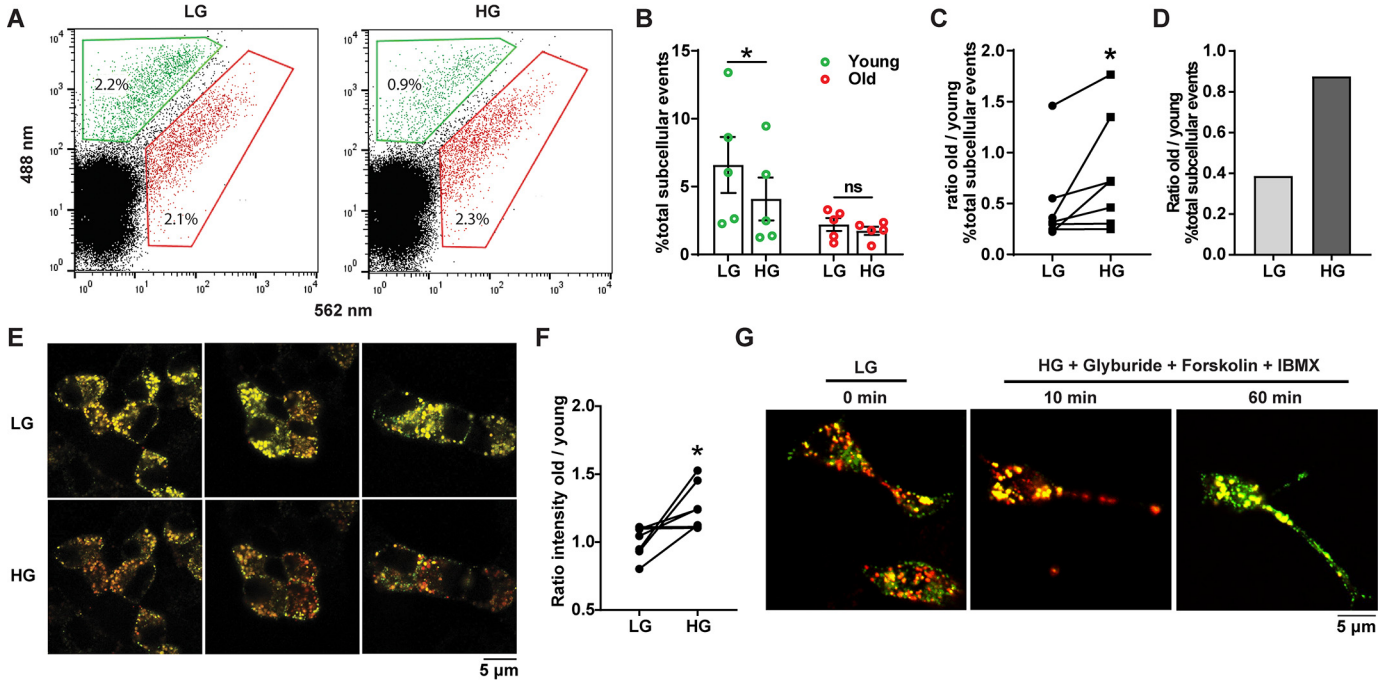

Figure 4. Flow cytometry-assisted organelle-sorting analysis of glucose-stimulated insulin secretion in primary mouse and human islets. *A*, FAOS analysis applied to dispersed mouse islets, 72 h post-transduction with syncollin-dsRedE5TIMER. Islet cells were pretreated at 2.8 mM glucose for 1 h and then treated for 10 min with 2.8 mM glucose (*LG*) or 16.7 mM glucose (*HG*). *B*, percentage of total young and old subcellular particles expressed as -fold change over 2.8 mM glucose (basal) after HG stimulation of dispersed mouse islets, 72 h post-transduction with syncollin-dsRedE5TIMER. *C* and *D*, ratio of the percentage of old subcellular particles over young subcellular particles in low- and high-glucose conditions after GSIS assay of dispersed mouse islets (*C*) and human islets (*D*), 72 h post-transduction with syncollin-dsRedE5TIMER. *, $p < 0.05$, one-way ANOVA with Tukey's multiple-comparison post-test. *E* and *F*, live-cell confocal imaging (*E*) and fluorescence intensity analysis (*F*) of fluorescing particles in MIN6 cells after a 10-min GSIS assay, 72 h post-transduction with syncollin-dsRedE5TIMER. *G*, live-cell confocal imaging of syncollin-dsRedE5TIMER–transduced INS1 cells, pretreated at 5.6 mM glucose for 1 h, and then stimulated with HG and 5 μM glyburide, 10 μM forskolin, and 1 mM IBMX at 10 and 60 min. *, $p = 0.02$, paired *t* test; *ns*, not significant.

syncollin-dsRedE5TIMER, dispersed mouse islet cells were subjected to 1 h of resting condition in KRBH buffer containing 2.8 mM glucose (basal) and then stimulated with KRBH containing either 2.8 mM glucose or 16.7 mM glucose. Immediately after stimulation, cells were lysed in 0.3 M sucrose in HEPES-EGTA buffer and processed for FAOS to analyze syncollin-dsRedE5TIMER–positive insulin SG populations. Paired analysis of treatments across eight separate experiments found a significantly increased ratio of old to young SGs remaining in cells post-stimulation with 16.7 mM glucose compared with 2.8 mM glucose (Fig. 4, *B* and *C*). FAOS analysis after high-glucose stimulation in human donor islets from one experiment also showed a preference for younger granule secretion (Fig. 4*D*).

Using live cell confocal imaging, preferential secretion of young SGs was also visualized in MIN6 cells. After a 1-h incubation at 2.8 mM glucose KRBH, cells were imaged 10 min after the addition of either 2.8 or 16.7 mM glucose KRBH (Fig. 4*E*). Regions of interest containing 3–8 cells were averaged across five experiments to obtain intensity values corresponding to the 505–550 nm and 590–700 nm emission spectra of young and old granules, respectively (Fig. 4*F*). As was observed with FAOS analysis of dispersed islets, 16.7 mM glucose stimulation resulted in an increased ratio of old to young granules retained in MIN6 cells, indicative of selective secretion biased toward younger granules. In live-cell imaging of syncollin-dsRedE5TIMER–transduced INS1 cells, selective young granule secretion was similarly observed. INS1 cells stimulated with 16.7 mM glucose and the addition of a "hyperstimulation mixture" of glyburide, forskolin, and 3-isobutyl-1-methylxanthine (IBMX) showed increased visible red fluorescence after 10 min of stimulation. More interestingly, 60 min post-stimulation, the reappearance of green fluorescence was observed, indicating replenishment of the young ISG pool (Fig. 4*G*).

These data together readily confirm (12–16) the occurrence of preferential secretion of younger insulin SG in both MIN6 and INS1 β-cells and dispersed mouse and human islet cells. Moreover, they highlight the phenomenon as glucose-regulated.

The β-cell environment alters the dynamics of young and old insulin SG populations

We next examined the relationship between SG age and the β-cell environment. Although there is evidence that newly synthesized insulin SGs are preferentially secreted upon stimulation under physiological conditions, it is not known how the changing environment of β-cells under metabolic stress affects the turnover and dynamics of age-distinct SG pools.

Islets were isolated from C57BL/6J WT mice and dispersed prior to transduction with syncollin-dsRedE5TIMER. After 24 h, culture medium was replaced with 2.8, 8.3, or 16.7 mM glucose RPMI to simulate a hypoglycemic, euglycemic, or hyperglycemic environment, respectively. After an additional 48-h culture period, islet cells were lysed for FAOS analysis. Healthy WT islets demonstrated a strikingly consistent phenotype in granule population age, with a significantly increased younger granule population observed in hyperglycemic conditions and, concomitantly, significantly reduced younger granules observed in hypoglycemic con-

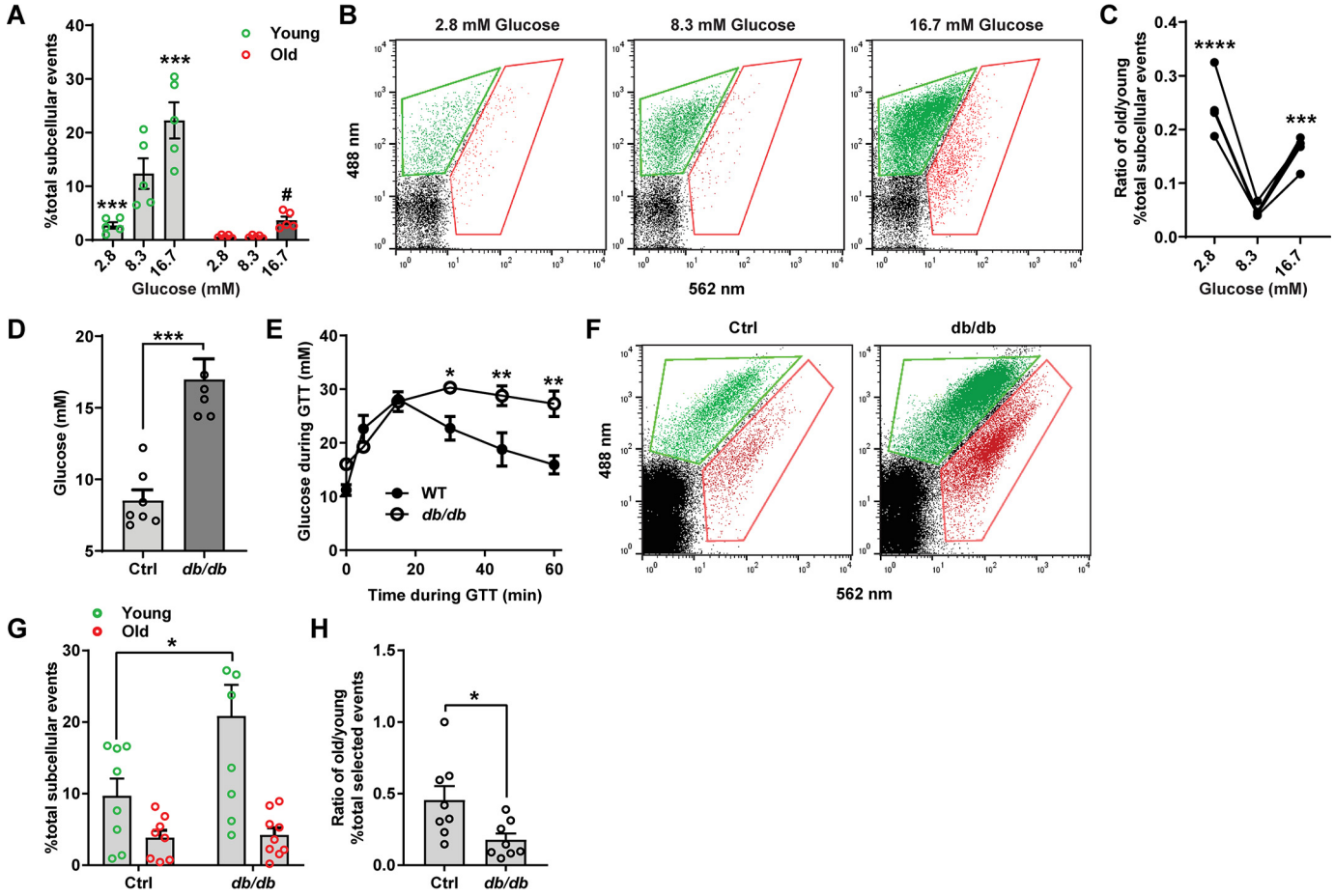

Figure 5. Young and old granule populations are modulated by the glucose environment in INS1 β-cells and primary mouse islets. *A*, young and old fluorescing particles defined as a percentage of total subcellular events were obtained from dispersed mouse islets. Islet cells were transduced with syncollin-dsRedE5TIMER for 24 h in 11 mM glucose RPMI and then placed in 2.8, 8.3, and 16.7 mM glucose RPMI for 48 h prior to processing for FAOS analysis. *B*, representative FAOS gating for young and old particles of dispersed islet cells at 2.8, 8.3, and 16.7 mM glucose conditions. *C*, ratio of the percentage of total old subcellular particles over the percentage of total young subcellular particles at 2.8, 8.3, and 16.7 mM glucose conditions. ***, $p < 0.001$; ****, $p < 0.0001$ compared with 8.3 mM glucose conditions, two-way ANOVA with Sidak's multiple-comparison tests. *D*, blood glucose measurements in littermate control (*Ctrl*) and *db/db* mice after a 5-h fast. Shown are pooled data from two litters. ***, $p < 0.001$, unpaired student's *t* test. *E*, blood glucose measurements during an intraperitoneal glucose tolerance test in one litter of *db/db* and littermate controls after a 5-h fast. *F*, representative FAOS gating for dispersed littermate control and *db/db* mice, 72 h post-transduction with syncollin-dsRedE5TIMER. *G* and *H*, percentage of total young and old subcellular particles (*G*) and ratio of percentage of total old over percentage of total young subcellular particles (*H*) in littermate control and *db/db* mice, 72 h post-transduction with syncollin-dsRedE5TIMER. Control and *db/db* mouse islets were recovered and dispersed into single islet cells in supplemented RPMI culture (11 mM glucose, "islet medium") conditions, with no glucose stimulation prior to FAOS analysis. *, $p < 0.05$, two-way ANOVA with Sidak's multiple-comparison test; **, $p < 0.01$, unpaired *t* test.

ditions (Fig. 5, *A* and *B*). At 16.7 mM glucose, the older granule population pool also increased. This consequently resulted in a higher old/young granule population ratio at both hypoglycemic and hyperglycemic conditions (Fig. 5*C*).

Next, we employed the leptin receptor–deficient *db/db* mouse model to assess granule behavior under conditions of β-cell dysfunction. *db/db* mice display severe obesity, glucose intolerance, hyperinsulinemia, and eventually hyperglycemia (37, 38). Prior to *in vitro* experiments, fasting glucose was obtained, and intraperitoneal glucose tolerance tests were performed to verify mutant obese *db/db* mice as diabetic (Fig. 5, *D* and *E*). Dispersed islet cells obtained from *db/db* mutant mice and their littermate controls were transduced with syncollin-dsRedE5TIMER and then lysed for FAOS analysis after 72 h. Across three litters, *db*/*db* mice exhibited higher percentages of younger granule populations compared with WT controls (Fig. 5, *F* and *G*), subsequently resulting in a significantly reduced old/young population ratio (Fig. 5*H*) and echoing the behavior observed previously in WT islets under chronic *in vitro* high-glucose environment. Together, these data demonstrate that the β-cell, under conditions of metabolic stress, is capable of highly subtle modulation of the intracellular SG population by age.

Discussion

Insulin SGs exist in distinctly behaving pools, some of which exhibit higher motility (14, 39) or enhanced membrane-docking properties (8) and others that are more prone to fusion with the plasma membrane (40, 41) or appear to be preferentially degraded (14, 42). By adding a temporal layer to these behaviors, we and others (14) have demonstrated that granule age is a key determinant of secretory preference.

By exploiting syncollin-dsRedE5TIMER's ability to traffic as an insulin SG cargo protein, we demonstrate that granule preference can occur in SGs as young as 24 h old (as syncollin-dsRedE5TIMER takes ~18 h to mature from green to red). These data are congruous with those previously described

using the SNAP tag reporter system (15), which defined younger granules as less than 5 h old and older granules as between 5 and 30 h in age, and have linked SG "youth" to increased motility, as well as secretory competency (43).

In the *db/db* mouse, increased immature SG biogenesis has previously been described as a result of β-cell compensatory responses (26). However, concomitant loss of functional secretory capacity is also observed (41) with a heightened β-cell workload resulting in increased ISG/proinsulin secretion as insulin granule maturation processes are unable to keep up with secretory demand. We similarly describe a significant increase in young or immature insulin SGs in our model of FAOS, validating the capacity of syncollin-dsRedE5TIMER to measure heightened insulin SG biogenesis in a model of β-cell dysfunction. It is important to note that the *db/db* mouse undergoes a significant period of β-cell compensation prior to β-cell failure, and it is possible that the elevated younger SG population observed in our *db/db* islets is a result of this compensatory response in the remaining β-cell. This is further evidenced by the fact that the C57BL6/J islet cells also display this significantly increased population. Accordingly, this compensatory behavior is reflected as high insulin turnover, which has previously been observed in *ex vivo* rat islets under hyperglycemic conditions of 16.7 mM glucose, which demonstrated increased insulin secretion coupled with significantly higher biosynthesis (16).

In the *db/db* mice, we also observed a smaller, but still evident, increase in the mature SG population. Similarly, we are also able to elicit an almost identical *in vitro* chronic hyperglycemic response from cultured WT islets, an increase in an aged granule population at 16.7 mM glucose. This mature SG persistence is likely a result of decreased intracellular insulin degradation when insulin secretion is high (21, 44), and it suggests that this compensatory mechanism is driven primarily by the hyperglycemic environment, as it appears conserved in both *ex vivo* models. Hypoglycemia also selectively reduced the young insulin SG population in our FAOS model but did not affect the older SG population. This is consistent with the observation that SG content is down-regulated in chronic starvation *in vivo* (45), whereas SG degradation pathways remain unaffected (16). Altogether, these data reinforce the dogma that β-cells exhibit functional adaptive flexibility to maintain homeostasis within environments of metabolic stress (45, 46) and suggest that insulin SG population age correlates with this flexibility.

We presently show that syncollin-dsRedE5TIMER is a valuable tool for this field, capable of distinguishing subtle granule dynamics within not just β-cell culture, but also the primary β-cell under both genetic and environmental perturbations. The application of FAOS with a fluorescent timer construct allows quantitative assessment of SG population age dynamics as well as the potential isolation of these populations for downstream transcript, proteomic, or lipidomic analyses. We note the temporal resolution of our model, which identifies older SGs as between 24 and 72 h old. At 24 h, insulin SGs are arguably still relatively young, but by 72 h, they are appreciably older than those previously investigated (15). The use of other fluorescent timers with different temporal qualities in this way will allow further interrogation of the properties behind insulin SG age and the metaphorical "switch" between youth and old age. There is evidence that younger SG motility mechanistically drives preferential secretion (14), and it could be speculated that the mobilization of these younger SGs may be driven by differential responses to intracellular calcium (39), but the reasons for granule selection bias remain unknown. Uncovering the necessity for this behavior within β-cells—how and why a β-cell determines insulin granule priority—may be key to developing therapies to rescue conditions of degranulation or β-cell dysfunction.

Experimental procedures

Cell culture

MIN6 cells were purchased from AddexBio (sourced from New Zealand), with passages less than 30 used in this study. GRINCH cells (36) were a gift from Professor Peter Arvan (University of Michigan). MIN6, INS1, and GRINCH were grown in Dulbecco's modified Eagle's medium and RPMI medium, respectively, supplemented with 10% fetal bovine serum, 2 mM L-glutamine, 20 mM HEPES, pH 7.4, 1 mM sodium pyruvate, 100 units/ml penicillin, and 100 μg/ml streptomycin. Cells were incubated at 37 °C, in humidified 95% air and 5% CO_2, and passaged every 3–4 days using TrypLE Express for 3 min at 37 °C. All cells were tested mycoplasma-negative, except for GRINCH cells used in preliminary data. All cell culture reagents were from Life Technologies, Inc.

Adenovirus syncollin-dsRedE5TIMER infection

Syncollin-dsRedE5TIMER was commercially amplified and characterized by ViraQuest, Inc. Cells or dispersed islets were infected with a 50–100 multiplicity of infection of Ad-syncollin-dsRedE5TIMER, respectively, in RPMI supplemented with 100 units/ml penicillin and 100 μg/ml streptomycin. After 24 h of transduction, cells were washed three times and then cultured in RPMI containing 10% fetal bovine serum, 100 units/ml penicillin, and 100 μg/ml streptomycin (islet medium). Fluorescence of granular structures at 490-nm excitation was typically visible from 12 h post-transduction.

Mice

Male C57BL/6J mice of 10–12 weeks were purchased from Australian BioResources. Mice were housed on a 12-h light/dark cycle in standard home cages in groups of up to six mice, with food and water given *ad libitum*. All procedures performed were in compliance with the National Health and Medical Research Council guidelines for animal research and approved by the University of Sydney Animal Ethics Committees. BKS.Cg-*Dock7m*+/+*Lepr*^{db}/J (*db/db*) mice were obtained from Garvan Institute breeding colonies (Australian BioResources, Moss Vale, New South Wales, Australia). Three litters of mice were used containing seven (two controls, five mutants), six (two controls, four mutants), and eight (five controls, two mutants) mice, respectively. Littermates were used in each experiment as controls. Mouse procedures were approved by the Garvan Institute/St. Vincent's Hospital Animal Experimentation Ethics Committee.

Human islets

Human islets were sourced from the Faculty of Medicine and Health (University of Sydney), the National Pancreas and Islet

Transplant Unit (NPITU), Westmead Hospital (Sydney, Australia), and the Islet Transplant Unit, St. Vincent's Hospital (Melbourne, Australia).

Approval for research use of human islets was obtained from the University of Sydney Human Research Ethics Committees (approval HREC 2017-042). All studies involving human samples abide by the Declaration of Helsinki principles.

Human pancreata were obtained, with informed consent from next of kin, from heart-beating, brain-dead donors. Human islets were purified by intraductal perfusion and digestion of the pancreas with collagenase followed by purification using Ficoll density gradients (47). Purified islets were cultured in Connaught Medical Research Laboratories (CMRL) 1066 medium (Invitrogen) supplemented with 4% human serum albumin, 100 units/ml penicillin, 100 mg/ml streptomycin, and 2 mM L-glutamine (complete CMRL), in a 37 °C, 5% CO_2 humidified incubator.

Mouse islets

Islets were isolated as described previously (30). Briefly, a 2-ml volume of 0.25 mg/ml Liberase (Roche Applied Science) in Hanks' buffered saline solution (Life Technologies) with 20 mM HEPES was injected into the common bile duct. The inflated pancreas was extracted, incubated at 37 °C for 13 min, and washed twice before passing through a 1,000-mm mesh filter. The resulting tissue was centrifuged with no break at 1,000 × *g* in a Histopaque 1119 and 1077 (Life Technologies) gradient for 20 min before islets were hand-picked in Hanks' buffered saline solution (Life Technologies).

For infection of C57Bl/6K and *db/db* mouse islets after isolation, islets were recovered in islet medium for 1 h, before infection with syncollin-dsRedE5TIMER for 24 h as stated above, and then washed three times and incubated in islet medium for another 48 h prior to analysis.

FAOS

Fluorescence-assisted organelle-sorting protocols were adapted from previous studies (32, 33) for β-cells. Islets were first dispersed by incubating in 100 μl of TrypLE Express (Thermo Fisher Scientific) for 3 min at 37 °C, pipetting up and down, before resuspension in islet medium for plating onto tissue culture dishes. Dispersed islets were infected with syncollin-dsRedE5TIMER as stated above and incubated for the indicated times. Cells were then scraped into 0.5 ml of PBS containing 0.3 M sucrose, 10 mM HEPES, and 0.25 mM EDTA (HEPES-EGTA buffer) and then passed 15 times each through a 21- and 25-gauge needle. The resulting homogenate was centrifuged at 1,000 × *g* for 5 min to remove intact cells, and the supernatant was diluted into 1.5 ml of PBS for flow cytometry sorting on an Influx 10 laser cell sorter (BD Biosciences) with a 70-μm filter, using 488- and 562-nm lasers. Calibration size reference beads (BD Biosciences) of 100 and 500 nm were used to determine size gate for insulin secretory granules, and 1 × 10^5 events within this gate were collected per sample, with the percentage of fluorescent particles normalized to total subcellular events from single-particle gated populations. Flow data were analyzed using FlowJo 10 software (BD Biosciences).

GSIS assay

Syncollin-dsRedE5TIMER–transduced cells were incubated for 1 h in basal conditions of Krebs–Ringer bicarbonate HEPES (KRBH buffer: 20 mM HEPES, pH 7.4, 119 mM NaCl, 4.75 mM KCl, 2.54 mM $CaCl_2$, 1.2 mM $MgSO_4$, 1.18 mM KH_2PO_4, 5 mM $NaHCO_3$) containing 2.8 mM glucose, before stimulation for 10 min in KBRH containing either 2.8 mM (low) glucose or 16.7 mM (high) glucose. Supernatant was removed, and cells were washed once in PBS before homogenization and analysis with FAOS. For measurements of secreted protein, GSIS was performed with a 1-h incubation in basal conditions as above, with 2.8 or 16.7 mM glucose stimulation for 2 h prior to the collection of supernatant from cells. Supernatant was measured for insulin secretion by an HTRF assay (Cisbio) or centrifuged at 1,000 × *g* to remove cellular debris and then precipitated with TCA (6% final concentration) in the presence of 0.02% sodium deoxycholate. Precipitate was washed in acetone and then resuspended into reducing Laemmli buffer for SDS-PAGE.

Glucose/glyburide/forskolin/IBMX experiment

INS-1 cells were grown on coverslips and transduced with syncollin-dsRedE5TIMER for 48 h in 5.6 mM glucose. At the time of infection, cells were ~30% confluent. At the end of 48 h, cells were incubated for 1 h in basal conditions of KRBH containing 2.8 mM glucose, before stimulation for 10 min in KBRH containing either 2.8 mM (low) glucose or hyperstimulation mixture of 16.7 mM glucose + 5 μM glyburide + 10 μM forskolin + 1 mM IBMX. Cells were fixed in 4% paraformaldehyde for 10 min and then mounted with AquaPolyMount and visualized with Olympus FV500 confocal imaging.

Taxol and brefeldin-A experiments

INS-1 cells were grown on coverslips and transduced with syncollin-dsRedE5TIMER for 48 h in 11 mM glucose. At the time of infection, cells were ~30% confluent. At the end of 48 h, cells were then incubated in KRBH containing 11 mM glucose plus 5 μM paclitaxel (Taxol, Sigma) or 10 μg/ml brefeldin A (Sigma) for 3 h. Cells were fixed in 4% paraformaldehyde for 15 min and then mounted with ProLong Diamond containing DAPI and visualized by confocal microscopy.

Subcellular fractionation and differential centrifugation

A continuous sucrose gradient was made from 2, 1.85, 1.6, 1.45, 1.2, 1.05, 0.9, 0.75, 0.6, and 0.45 M sucrose in HEPES-EGTA buffer (10 mM HEPES, 0.25 mM EGTA) and left to equilibrate at 4 °C overnight. Syncollin-dsRedE5TIMER–transduced cells were lysed via needle pulse (10 × 19-gauge needle, 10 × 25-gauge needle) in 0.3 M sucrose, 10 mM HEPES, 0.25 mM EGTA. The resulting homogenate was centrifuged for 5 min at 1,000 × *g*, and the supernatant was loaded onto the top of the continuous sucrose gradient and centrifuged at 50,000 × *g* for 18 h at 4 °C. 13 fractions were collected and were diluted 1:4 into reducing 4× Laemmli buffer for SDS-PAGE.

Immunofluorescent staining

MIN6 cells were seeded onto 1.5-mm coverslips within 6-well plates 24 h prior to syncollin-dsRedE5TIMER transduc-

tion. Cells were fixed in 4% paraformaldehyde and washed twice with PBS before antigen retrieval was performed with 0.1% SDS for 5 min at room temperature. After washing twice with PBS containing 0.1% BSA and 0.01% Triton X-100, cells were blocked for 1 h at room temperature with Protein Block (Agilent DAKO, Santa Clara, CA) and then incubated in a humidified chamber overnight with guinea pig anti-insulin antibody at 1:1,000 dilution (DAKO). The following day, cells were washed twice with PBS containing 0.1% BSA and 0.01% Triton X-100, incubated for 1 h at room temperature with anti-guinea pig secondary, washed three times, and mounted onto microscope slides with ProLong Diamond containing DAPI.

Microscopy

Fixed slides and live cell dishes were both imaged using a Leica LCS SP8 confocal microscope (Wetzlar, Germany), using a white light laser and ×100 magnification oil lens. Images were collected using Leica LAS X software and analyzed using Fiji ImageJ software (35).

Fixed slides were imaged for TIRF microscopy using a Nikon H-TIRF module with an argon laser (488 nm, 561 nm) and ×60 magnification oil lens. The illumination angle was set to ~110 nm. Images were collected using NIS Elements software.

Statistical analysis

Data analyses were performed using GraphPad Prism 7 and 8 software. Statistical significance was set at $p < 0.05$. p values were calculated using Student's t test, Tukey's multiple-comparison post-test in one-way ANOVA, or Sidak's multiple-comparison post-test in two-way ANOVA, where indicated. Data are expressed as mean ± S.E.

Data availability

All data are contained within the article or available upon request of the corresponding author, Melkam A. Kebede.

Acknowledgments—We thank Professor David E. James and his research group (University of Sydney) for insightful discussions. We thank all organ donors and their families for their generosity and for enabling this work. We thank the staff of St. Vincent's Institute (Melbourne) and Westmead Hospital (Sydney) involved in the islet isolation program and Donatelife for obtaining research consent and providing the human pancreata. Human tissue retrieval was supported by the Operational Infrastructure Support Scheme of the Government of Victoria. We acknowledge the facilities and the scientific and technical assistance of the Australian Microscopy and Microanalysis Research Facility at Sydney Microscopy and Microanalysis, University of Sydney, and Sydney Cytometry Facility, University of Sydney and Centenary Institute.

Author contributions—B. Y., L. H., C. L., and D. R. L. data curation; B. Y., L. H., C. L., D. R. L., and M. A. K. formal analysis; B. Y., L. H., P. T., C. J. R., and M. A. K. methodology; B. Y. writing-original draft; B. Y. and M. A. K. project administration; L. H. and M. A. K. investigation; H. E. T., J. E. G., L. W., W. J. H., C. J. R., and M. A. K. resources; P. T. and M. A. K. supervision; P. T. and M. A. K. funding acquisition; M. A. K. conceptualization; M. A. K. writing-review and editing.

Funding and additional information—The work was supported by National Health and Medical Research Council (NHMRC) of Australia Grant GNT1139828. M. A. K. is supported by a Jennie Mackenzie Philanthropic Fellowship, University of Sydney.

Conflict of interest—CJR is a current employee of AstraZeneca and owns stock in the company.

Abbreviations—The abbreviations used are: GSIS, glucose-stimulated insulin secretion; SG, secretory granule; ISG, insulin SG; HTRF, homogeneous time-resolved fluorescence; FAOS, flow cytometer–assisted organelle sorting; IBMX, 3-isobutyl-1-methylxanthine; DAPI, 4′,6-diamidino-2-phenylindole; TIRF, total internal reflection fluorescence; ANOVA, analysis of variance.

References

1. Barg, S., Eliasson, L., Renström, E., and Rorsman, P. (2002) A subset of 50 secretory granules in close contact with L-type Ca^{2+} channels accounts for first-phase insulin secretion in mouse beta-cells. *Diabetes* **51,** S74–S82 CrossRef Medline
2. Rorsman, P., Eliasson, L., Renström, E., Gromada, J., Barg, S., and Göpel, S. (2000) The cell physiology of biphasic insulin secretion. *News Physiol. Sci.* **15,** 72–77 Medline
3. Henquin, J. C., Ishiyama, N., Nenquin, M., Ravier, M. A., and Jonas, J. C. (2002) Signals and pools underlying biphasic insulin secretion. *Diabetes* **51,** S60–S67 CrossRef Medline
4. Gaisano, H. Y. (2014) Here come the newcomer granules, better late than never. *Trends Endocrinol. Metab.* **25,** 381–388 CrossRef Medline
5. Hanna, S. T., Pigeau, G. M., Galvanovskis, J., Clark, A., Rorsman, P., and MacDonald, P. E. (2009) Kiss-and-run exocytosis and fusion pores of secretory vesicles in human beta-cells. *Pflugers Arch.* **457,** 1343–1350 CrossRef Medline
6. Tsuboi, T., Zhao, C., Terakawa, S., and Rutter, G. A. (2000) Simultaneous evanescent wave imaging of insulin vesicle membrane and cargo during a single exocytotic event. *Curr. Biol.* **10,** 1307–1310 CrossRef Medline
7. Do, O. H., Gunton, J. E., Gaisano, H. Y., and Thorn, P. (2016) Changes in beta cell function occur in prediabetes and early disease in the Lepr (db) mouse model of diabetes. *Diabetologia* **59,** 1222–1230 CrossRef Medline
8. Kasai, K., Fujita, T., Gomi, H., and Izumi, T. (2008) Docking is not a prerequisite but a temporal constraint for fusion of secretory granules. *Traffic* **9,** 1191–1203 CrossRef Medline
9. Gold, G., Gishizky, M. L., and Grodsky, G. M. (1982) Evidence that glucose "marks" beta cells resulting in preferential release of newly synthesized insulin. *Science* **218,** 56–58 CrossRef Medline
10. Howell, S. L., and Taylor, K. W. (1967) The secretion of newly synthesized insulin *in vitro*. *Biochem. J.* **102,** 922–927 CrossRef Medline
11. Rhodes, C. J., and Halban, P. A. (1987) Newly synthesized proinsulin/insulin and stored insulin are released from pancreatic B cells predominantly via a regulated, rather than a constitutive, pathway. *J. Cell Biol.* **105,** 145–153 CrossRef Medline
12. Hou, N., Mogami, H., Kubota-Murata, C., Sun, M., Takeuchi, T., and Torii, S. (2012) Preferential release of newly synthesized insulin assessed by a multi-label reporter system using pancreatic beta-cell line MIN6. *PLoS ONE* **7,** e47921 CrossRef Medline
13. Duncan, R. R., Greaves, J., Wiegand, U. K., Matskevich, I., Bodammer, G., Apps, D. K., Shipston, M. J., and Chow, R. H. (2003) Functional and spatial segregation of secretory vesicle pools according to vesicle age. *Nature* **422,** 176–180 CrossRef Medline
14. Hoboth, P., Müller, A., Ivanova, A., Mziaut, H., Dehghany, J., Sönmez, A., Lachnit, M., Meyer-Hermann, M., Kalaidzidis, Y., and Solimena, M. (2015) Aged insulin granules display reduced microtubule-dependent mobility and are disposed within actin-positive multigranular bodies. *Proc. Natl. Acad. Sci. U.S.A.* **112,** E667–E676 CrossRef Medline
15. Ivanova, A., Kalaidzidis, Y., Dirkx, R., Sarov, M., Gerlach, M., Schroth-Diez, B., Müller, A., Liu, Y., Andree, C., Mulligan, B., Münster, C., Kurth,

T., Bickle, M., Speier, S., Anastassiadis, K., and Solimena, M. (2013) Age-dependent labeling and imaging of insulin secretory granules. *Diabetes* **62,** 3687–3696 CrossRef Medline

16. Halban, P. A. (1982) Differential rates of release of newly synthesized and of stored insulin from pancreatic islets. *Endocrinology* **110,** 1183–1188 CrossRef Medline
17. Ohara-Imaizumi, M., Nishiwaki, C., Kikuta, T., Nagai, S., Nakamichi, Y., and Nagamatsu, S. (2004) TIRF imaging of docking and fusion of single insulin granule motion in primary rat pancreatic beta-cells: different behaviour of granule motion between normal and Goto-Kakizaki diabetic rat beta-cells. *Biochem. J.* **381,** 13–18 CrossRef Medline
18. Ohara-Imaizumi, M., Fujiwara, T., Nakamichi, Y., Okamura, T., Akimoto, Y., Kawai, J., Matsushima, S., Kawakami, H., Watanabe, T., Akagawa, K., and Nagamatsu, S. (2007) Imaging analysis reveals mechanistic differences between first- and second-phase insulin exocytosis. *J. Cell Biol.* **177,** 695–705 CrossRef Medline
19. Shibasaki, T., Takahashi, H., Miki, T., Sunaga, Y., Matsumura, K., Yamanaka, M., Zhang, C., Tamamoto, A., Satoh, T., Miyazaki, J., and Seino, S. (2007) Essential role of Epac2/Rap1 signaling in regulation of insulin granule dynamics by cAMP. *Proc. Natl. Acad. Sci. U.S.A.* **104,** 19333–19338 CrossRef Medline
20. Yasuda, T., Shibasaki, T., Minami, K., Takahashi, H., Mizoguchi, A., Uriu, Y., Numata, T., Mori, Y., Miyazaki, J., Miki, T., and Seino, S. (2010) Rim2α determines docking and priming states in insulin granule exocytosis. *Cell Metab.* **12,** 117–129 CrossRef Medline
21. Halban, P. A., and Wollheim, C. B. (1980) Intracellular degradation of insulin stores by rat pancreatic islets *in vitro*: an alternative pathway for homeostasis of pancreatic insulin content. *J. Biol. Chem.* **255,** 6003–6006 Medline
22. Dean, P. M. (1973) Ultrastructural morphometry of the pancreatic cell. *Diabetologia* **9,** 115–119 CrossRef Medline
23. Olofsson, C. S., Göpel, S. O., Barg, S., Galvanovskis, J., Ma, X., Salehi, A., Rorsman, P., and Eliasson, L. (2002) Fast insulin secretion reflects exocytosis of docked granules in mouse pancreatic B-cells. *Pflugers Arch.* **444,** 43–51 CrossRef Medline
24. Marsh, B. J., Soden, C., Alarcón, C., Wicksteed, B. L., Yaekura, K., Costin, A. J., Morgan, G. P., and Rhodes, C. J. (2007) Regulated autophagy controls hormone content in secretory-deficient pancreatic endocrine beta-cells. *Mol. Endocrinol.* **21,** 2255–2269 CrossRef Medline
25. Logothetopoulos, J., Davidson, J. K., Haist, R. E., and Best, C. H. (1965) Degranulation of beta cells and loss of pancreatic insulin after infusions of insulin antibody or glucose. *Diabetes* **14,** 493–500 CrossRef Medline
26. Alarcon, C., Boland, B. B., Uchizono, Y., Moore, P. C., Peterson, B., Rajan, S., Rhodes, O. S., Noske, A. B., Haataja, L., Arvan, P., Marsh, B. J., Austin, J., and Rhodes, C. J. (2016) Pancreatic beta-cell adaptive plasticity in obesity increases insulin production but adversely affects secretory function. *Diabetes* **65,** 438–450 CrossRef Medline
27. Like, A. A., and Chick, W. L. (1970) Studies in the diabetic mutant mouse. II. Electron microscopy of pancreatic islets. *Diabetologia* **6,** 216–242 CrossRef Medline
28. Terskikh, A., Fradkov, A., Ermakova, G., Zaraisky, A., Tan, P., Kajava, A. V., Zhao, X., Lukyanov, S., Matz, M., Kim, S., Weissman, I., and Siebert, P. (2000) "Fluorescent timer": protein that changes color with time. *Science* **290,** 1585–1588 CrossRef Medline
29. Tsuboi, T., Kitaguchi, T., Karasawa, S., Fukuda, M., and Miyawaki, A. (2010) Age-dependent preferential dense-core vesicle exocytosis in neuroendocrine cells revealed by newly developed monomeric fluorescent timer protein. *Mol. Biol. Cell* **21,** 87–94 CrossRef Medline
30. Kebede, M. A., Oler, A. T., Gregg, T., Balloon, A. J., Johnson, A., Mitok, K., Rabaglia, M., Schueler, K., Stapleton, D., Thorstenson, C., Wrighton, L., Floyd, B. J., Richards, O., Raines, S., Eliceiri, K., *et al.* (2014) SORCS1 is necessary for normal insulin secretory granule biogenesis in metabolically stressed beta cells. *J. Clin. Invest.* **124,** 4240–4256 CrossRef Medline
31. Hays, L. B., Wicksteed, B., Wang, Y., McCuaig, J. F., Philipson, L. H., Edwardson, J. M., and Rhodes, C. J. (2005) Intragranular targeting of syncollin, but not a syncollinGFP chimera, inhibits regulated insulin exocytosis in pancreatic β-cells. *J. Endocrinol.* **185,** 57–67 CrossRef Medline
32. Varadi, A., Tsuboi, T., and Rutter, G. A. (2005) Myosin Va transports dense core secretory vesicles in pancreatic MIN6 beta-cells. *Mol. Biol. Cell* **16,** 2670–2680 CrossRef Medline
33. Gauthier, D. J., Sobota, J. A., Ferraro, F., Mains, R. E., and Lazure, C. (2008) Flow cytometry-assisted purification and proteomic analysis of the corticotropes dense-core secretory granules. *Proteomics* **8,** 3848–3861 CrossRef Medline
34. Mirabella, R., Franken, C., van der Krogt, G. N., Bisseling, T., and Geurts, R. (2004) Use of the fluorescent timer DsRED-E5 as reporter to monitor dynamics of gene activity in plants. *Plant Physiol.* **135,** 1879–1887 CrossRef Medline
35. Schindelin, J., Arganda-Carreras, I., Frise, E., Kaynig, V., Longair, M., Pietzsch, T., Preibisch, S., Rueden, C., Saalfeld, S., Schmid, B., Tinevez, J. Y., White, D. J., Hartenstein, V., Eliceiri, K., Tomancak, P., and Cardona, A. (2012) Fiji: an open-source platform for biological-image analysis. *Nat. Methods* **9,** 676–682 CrossRef Medline
36. Haataja, L., Snapp, E., Wright, J., Liu, M., Hardy, A. B., Wheeler, M. B., Markwardt, M. L., Rizzo, M., and Arvan, P. (2013) Proinsulin intermolecular interactions during secretory trafficking in pancreatic beta cells. *J. Biol. Chem.* **288,** 1896–1906 CrossRef Medline
37. Chen, H., Charlat, O., Tartaglia, L. A., Woolf, E. A., Weng, X., Ellis, S. J., Lakey, N. D., Culpepper, J., Moore, K. J., Breitbart, R. E., Duyk, G. M., Tepper, R. I., and Morgenstern, J. P. (1996) Evidence that the diabetes gene encodes the leptin receptor: identification of a mutation in the leptin receptor gene in db/db mice. *Cell* **84,** 491–495 CrossRef Medline
38. Friedman, J. M., and Halaas, J. L. (1998) Leptin and the regulation of body weight in mammals. *Nature* **395,** 763–770 CrossRef Medline
39. Hao, M., Li, X., Rizzo, M. A., Rocheleau, J. V., Dawant, B. M., and Piston, D. W. (2005) Regulation of two insulin granule populations within the reserve pool by distinct calcium sources. *J. Cell Sci.* **118,** 5873–5884 CrossRef Medline
40. Nagamatsu, S., Bolaffi, J. L., and Grodsky, G. M. (1987) Direct effects of glucose on proinsulin synthesis and processing during desensitization. *Endocrinology* **120,** 1225–1231 CrossRef Medline
41. Zhu, D., Koo, E., Kwan, E., Kang, Y., Park, S., Xie, H., Sugita, S., and Gaisano, H. Y. (2013) Syntaxin-3 regulates newcomer insulin granule exocytosis and compound fusion in pancreatic beta cells. *Diabetologia* **56,** 359–369 CrossRef Medline
42. Pasquier, A., Vivot, K., Erbs, E., Spiegelhalter, C., Zhang, Z., Aubert, V., Liu, Z., Senkara, M., Maillard, E., Pinget, M., Kerr-Conte, J., Pattou, F., Marciniak, G., Ganzhorn, A., Ronchi, P., *et al.* (2019) Lysosomal degradation of newly formed insulin granules contributes to beta cell failure in diabetes. *Nat. Commun.* **10,** 3312 CrossRef Medline
43. Fava, E., Dehghany, J., Ouwendijk, J., Müller, A., Niederlein, A., Verkade, P., Meyer-Hermann, M., and Solimena, M. (2012) Novel standards in the measurement of rat insulin granules combining electron microscopy, high-content image analysis and *in silico* modelling. *Diabetologia* **55,** 1013–1023 CrossRef Medline
44. Uchizono, Y., Alarcón, C., Wicksteed, B. L., Marsh, B. J., and Rhodes, C. J. (2007) The balance between proinsulin biosynthesis and insulin secretion: where can imbalance lead? *Diabetes Obes. Metab.* **9,** 56–66 CrossRef Medline
45. Boland, B. B., Brown, C., Jr, Alarcon, C., Demozay, D., Grimsby, J. S., and Rhodes, C. J. (2018) β-Cell control of insulin production during starvation-refeeding in male rats. *Endocrinology* **159,** 895–906 CrossRef Medline
46. Kang, T., Boland, B. B., Alarcon, C., Grimsby, J. S., Rhodes, C. J., and Larsen, M. R. (2019) Proteomic analysis of restored insulin production and trafficking in obese diabetic mouse pancreatic islets following euglycemia. *J. Proteome Res.* **18,** 3245–3258 CrossRef Medline
47. Hawthorne, W. J., Williams, L., and Chew, Y. V. (2016) Clinical islet isolation. *Adv Exp. Med. Biol.* **938,** 89–122 CrossRef Medline